

Accepted on 2014 December 11 for publication in the Astrophysical Journal Letters

**Dust from Comet 209P/LINEAR during its 2014 Return:
Parent Body of a New Meteor Shower, the May Camelopardalids**

Masateru ISHIGURO[†]

*Department of Physics and Astronomy, Seoul National University, Gwanak, Seoul 151-742,
South Korea*

Daisuke KURODA

*Okayama Astrophysical Observatory, National Astronomical Observatory of Japan,
Asakuchi, Okayama 719-0232, Japan*

Hidekazu HANAYAMA

*Ishigakijima Astronomical Observatory, National Astronomical Observatory of Japan,
Ishigaki, Okinawa 907-0024, Japan*

Jun TAKAHASHI

*Nishi-Harima Astronomical Observatory, Center for Astronomy, University of Hyogo,
Sayo, Hyogo 679-5313, Japan*

Sunao HASEGAWA, Yuki SARUGAKU

*Institute of Space and Astronautical Science (ISAS), Japan Aerospace Exploration Agency
(JAXA), Sagami-hara, Kanagawa 252-5210, Japan*

Makoto WATANABE, Masataka IMAI, Shuhei GODA

*Department of CosmoSciences, Graduate School of Science, Hokkaido University, Sapporo
060-0810, Japan*

Hiroshi AKITAYA

*Hiroshima Astrophysical Science Center, Hiroshima University, Higashihiroshima,
Hiroshima 739-8526, Japan*

Yuhei TAKAGI, Kumiko MORIHANA, Satoshi HONDA, Akira ARAI

*Nishi-Harima Astronomical Observatory, Center for Astronomy, University of Hyogo,
Sayo, Hyogo 679-5313, Japan*

Kazuhiro SEKIGUCHI

*National Astronomical Observatory of Japan, National Institute of Natural Sciences,
Mitaka, Tokyo 181-8588, Japan*

Yumiko OASA

Faculty of Education, Saitama University, Sakura, Saitama 338-8570, Japan

Yoshihiko SAITO

Department of Physics, Tokyo Institute of Technology, Meguro-ku, Tokyo 152-8551, Japan

Tomoki MOROKUMA

*Institute of Astronomy, Graduate School of Science, The University of Tokyo, Mitaka,
Tokyo 181-0015, Japan*

Katsuhiko MURATA

Department of Astrophysics, Nagoya University, Chikusa-ku, Nagoya 464-8602, Japan

Daisaku NOGAMI

*Department of Astronomy, Graduate School of Science, Kyoto University, Kyoto 606-8502,
Japan*

Takahiro NAGAYAMA

*Graduate School of Science and Engineering, Kagoshima University, Kagoshima 890-0065,
Japan*

Kenshi YANAGISAWA

*Okayama Astrophysical Observatory, National Astronomical Observatory of Japan,
Asaguchi, Okayama 719-0232, Japan*

Michitoshi YOSHIDA

*Hiroshima Astrophysical Science Center, Hiroshima University, 1-3-1 Kagamiyama,
Higashi-Hiroshima, Hiroshima 739-8526, Japan*

Kouji OHTA

Department of Astronomy, Kyoto University, Kyoto 606-8502, Japan

Nobuyuki KAWAI

Department of Physics, Tokyo Institute of Technology, Meguro-ku, Tokyo 152-8551, Japan

Takeshi MIYAJI

*Ishigakijima Astronomical Observatory, National Astronomical Observatory of Japan,
Ishigaki, Okinawa 907-0024, Japan*

Hideo FUKUSHIMA, Jun-ichi WATANABE

National Astronomical Observatory of Japan, Mitaka, Tokyo 181-8588, Japan

Cyrielle OPITOM, Emmanuël JEHIN, Michael GILLON

*Institut d’Astrophysique de l’Université de Liège, Allée du 6 Août 17, B-4000 Liège,
Belgium*

Jeremie J. VAUBAILLON

Observatoire de Paris, I.M.C.C.E., Denfert Rochereau, Bat. A., FR-75014 Paris, France

ABSTRACT

We report a new observation of the Jupiter-family comet 209P/LINEAR during its 2014 return. The comet is recognized as a dust source of a new meteor shower, the May Camelopardalids. 209P/LINEAR was apparently inactive at a heliocentric distance $r_h = 1.6$ au and showed weak activity at $r_h \leq 1.4$ au. We found an active region of $<0.001\%$ of the entire nuclear surface during the comet’s dormant phase. An edge-on image suggests that particles up to 1 cm in size (with an uncertainty of factor 3–5) were ejected following a differential power-law size distribution with index $q = -3.25 \pm 0.10$. We derived a mass loss rate of 2–10 kg sec⁻¹ during the active phase and a total mass of $\approx 5 \times 10^7$ kg during the 2014 return. The ejection terminal velocity of millimeter- to centimeter-sized particles was 1–4 m sec⁻¹, which is comparable to the escape velocity from the nucleus (1.4 m sec⁻¹). These results imply that such large meteoric particles marginally escaped from the highly dormant comet nucleus via the gas drag force only within a few months of the perihelion passage.

[†]Visiting Astronomer, Observatoire de Paris, I.M.C.C.E., Denfert Rochereau, Bat. A., FR-75014 Paris, France, in 2014 May–July

Subject headings: comets: individual (209P/LINEAR) — interplanetary medium
 — meteorites, meteors, meteoroids

1. Introduction

The link between comets and meteor showers is important for better understanding of how pristine cometary materials have been delivered to the Earth. 209P/LINEAR (hereafter 209P) has an orbit typical of Jupiter-family comets, that is, a semimajor axis $a=2.932$ au, eccentricity $e=0.692$, inclination $i=19.4^\circ$, and Tisserand parameter with respect to Jupiter, T_J , of 2.80. It was suggested that a swarm of dust from 209P might cause a meteor shower on UT 2014 May 24 (Jenniskens & Lyytinen 2014). Ye & Wiegert (2014) has reported that 209P is relatively depleted in dust production, with a low level of activity around the perihelion passage in 2008–2009. This paper attempts to characterize the physical properties further through a new observation in 2014. We focus on the dust ejection properties (e.g., particle size and ejection terminal velocity), which are pivotal for linking the comet with the meteor shower via a dynamical model (see, e.g., Vaubaillon & Colas 2005).

2. Observations and Date Analysis

The journal of these observations is summarized in Table 1. The first imaging observation was conducted on UT 2014 February 1 using a Tektronix 2048×2048 pixel CCD camera (Tek2k) on the University of Hawaii 2.24-m telescope (UH2.2m) atop Mauna Kea. We obtained optical images with a broadband Kron–Cousins R_C -band filter. We noticed that the comet appeared point-like even at a heliocentric distance $r_h = 1.57$ au, where comets generally display comae and tails. Later, we made a network observation through the Optical and Infrared Synergetic Telescopes for Education and Research (*OISTER*), which is an inter-university observation network in the optical and infrared wavelengths. Among the *OISTER* network, we used four telescopes for the present study: the Nishi-Harima Astronomical Observatory Nayuta 2.0-m telescope (NHAO2m), the Ishigakijima Astronomical Observatory Murikabushi 1.0-m telescope (IAO1m), the Okayama Astrophysical Observatory 0.5-m reflecting telescope (OAO0.5m), and the Nayoro Observatory 1.6-m Pirka telescope of the Hokkaido University (NO1.6m). We employed the optical imaging cameras MINT (a back-illuminated 2048×2064 CCD chip with a $15\text{-}\mu\text{m}$ pixel pitch) with R_C - and I_C -band filters at NHAO2m, two sets of MITSuME (g' , R_C , and I_C -band simultaneous imaging system, a 1024×1024 CCD chip with a $24.0\text{-}\mu\text{m}$ pixel pitch) at IAO1m and OAO0.5m, and the MSI (a visible multispectral imager with a 512×512 CCD chip with a $16.0\text{-}\mu\text{m}$

pixel pitch (Watanabe et al. 2012) at NO1.6m. The two sets of MITSuME at IAO1m and OAO0.5m were designed identically, and each houses three front-illuminated CCD cameras. After early June 2014, 209P was unobservable from these observatories, which are located in the northern hemisphere. Instead, we observed the comet with the 0.6-m Transiting Planets and Planetesimals Small Telescope (TRAPPIST0.6m) with a 2048×2048 back-illuminated CCD chip with a $15\text{-}\mu\text{m}$ pixel pitch (Jehin et al. 2011). It covers $22' \times 22'$ with a resolution of $1.3'' \text{ pixel}^{-1}$ using 2×2 binning. All telescopes were operated in a non-sidereal tracking mode so that the comet was stationary in the observed frames.

The observed data were analyzed in the standard manner for optical and near-infrared imaging data. We constructed median-stacked frames using 209P frames or dome flat images to correct for the effect of the pixel-to-pixel sensitivity variations across the detectors as well as optical vignetting (what is called the flat field image). The photometric zero levels were determined using Landolt photometric standard stars (Landolt 1992) for UH88 and NO1.6m data and field stars listed in the USNO-A2.0 catalog (Mothé-Diniz et al. 2003) for the others. The images observed during a single night were combined to confirm the existence of a dust coma and further investigate the surface brightness profile of the dust tail (see Section 3.4).

3. Results

3.1. Appearance

We found no significant morphological differences between the g' -, R_C - and I_C -band images taken with MITSuME. The obtained color indices, $g' - R_C = 0.8 \pm 0.3$ and $R_C - I_C = 0.5 \pm 0.3$, are consistent with those of the Sun, that is, $(g' - R_C)_\odot = 0.65$ (Kim et al. 2012) and $(R_C - I_C)_\odot = 0.33$ (Holmberg et al. 2006), which implies that the reflected light from the nucleus and dust are the dominant light sources of the detected intensity. In addition, it is reported that the spectrum taken with the 8-m Gemini North telescope on April 9.25 UT did not reveal obvious emission lines attributable to sources such as C_2 around $4500\text{--}5600\text{\AA}$ and NH_2 around $4900\text{--}6300\text{\AA}$ (Schleicher 2014). For these reasons, we ignored the contribution of gaseous emission in our R_C -band data and used the R_C -band magnitudes for the subsequent photometric analysis (see also Table 1).

Figure 1 shows selected R_C -band images of 209P. In the first image, taken on UT 2014 February 1 (at $r_h = 1.57$ au), neither the coma nor the dust tail was visually apparent. An unclear tail-like feature extended to the position angle (the angle on the celestial plane measured from north through east) $PA \sim 185^\circ$. It is not clear whether the feature was attributable to the cometary tail or an artifact such as a diffraction spike from the support vanes of the

secondary mirror. The $1.05''$ – $1.06''$ full width at half-maximum (FWHM) of the field stars is in perfect agreement with the value of $1.05''$ in the combined 209P image. In Figure 2 (a), we compare the radial profile of 209P in a composite image with that of a field star taken in sidereal tracking mode between the 209P exposures. We found that the surface brightness profiles coincided with one another at the 10^{-3} – $10^{-2}\%$ level of the photocenter. The similarity suggests that the comet was highly dormant on that night (UT 2014 February 01). We set an upper limit of 0.01 for the parameter η , which is defined as the ratio of the coma cross section to the nucleus cross section. Adopting a model in Luu & Jewitt (1992) and assuming the ejection of small dust particles (a radius of $a_d=0.5 \mu\text{m}$) that are embedded in surface water ice, we obtained approximate estimates for the dust production rate $M_d \lesssim 0.01 \text{ kg s}^{-1}$ and the fractional active area $f \lesssim 1 \times 10^{-5}$ on UT 2014 February 1 (see also Ishiguro et al. 2011). The obtained f value is significantly lower than those of the typical Jupiter-family comets ($f > 10^{-3}$, Tancredi et al. 2006).

In Figure 1 (b) (UT 2013 March 03 at $r_h=1.30 \text{ au}$), the comet still appeared point-like. However, a careful investigation revealed a faint tail-like structure extending to $\text{PA}=128\pm 3^\circ$, which is close to the position angles of the Sun–comet radius vector ($\text{PA}=123^\circ$) but deviates slightly to the negative heliocentric velocity vector ($\text{PA}=216^\circ$). Since cometary dust tails usually appear between these two vectors, and the position angle does not align with the diffraction spike caused by the secondary mirror, we suspect that the extended structure might be a real cometary tail. In Figure 1 (c) (UT 2013 March 23), the cometary tail was clearly detected. It extended to $\text{PA}=105\pm 4^\circ$, existing between the antisolar direction ($\text{PA}=100^\circ$) and the negative heliocentric velocity vector ($\text{PA}=193^\circ$). We detected an obvious tail in all the images after UT 2013 March 22. Figure 1 (d) was taken when the comet was viewed edge-on on UT 2013 May 23. Note that the image was rotated to align the projected orbital plane in the horizontal direction. The comet possessed a narrow tail extended to $\text{PA}=108\pm 1^\circ$, which coincided with the position angle of the orbital plane projected on the sky ($\text{PA}=107.4^\circ$). The tail extended out of the FOV (i.e., $>13''$). Further, the dust cloud extended sunward by $30''$ (rightward in the image), probably because of the ejection of fresh dust particles toward the Sun. To obtain a crude estimate of the ejection velocity, we employed the formula $l = v_{ej}^2 / (2\beta g_\odot)$, where l is the apparent length of the sunward tail, v_{ej} is the terminal escape velocity of dust particles, β is the ratio of the solar radiation pressure to the solar gravity, and g_\odot is the solar gravity at the position of the comet (Jewitt & Meech 1987). We obtained 1.1 m sec^{-1} assuming 1-cm particles and 3.4 m sec^{-1} assuming 1-mm particles. The order of magnitude estimate for v_{ej} is consistent with the result of another model described below (Section 3.4).

3.2. Properties of Nucleus

Figure 2 (b) shows the lightcurves of 209P measured from each image on UT 2014 February 1. The data were calibrated using Landolt photometric standard stars, ensuring an absolute magnitude accuracy of 0.05 mag or less (Landolt 1992). The rotational lightcurve covered one peak and probably two troughs (both ends), suggesting that the rotational period is not shorter than the observational duration (7 h). The inferred rotational period is consistent with a report by Hergenrother in which he derived two alternative solutions of 10.930 ± 0.015 and 21.86 ± 0.04 h (Green 2014). We calculated the corresponding amplitude at $\alpha = 0^\circ$ using an empirical function (Zappala et al. 1990),

$$A(0) = \frac{A(\alpha)}{1 + m\alpha}, \quad (1)$$

where $A(0^\circ)$ and $A(\alpha)$ are the amplitudes at phase angles (Sun–comet–observer angles) of 0° and α , respectively, and m is a correction coefficient for the amplitude, which has different values for S-, C-, and M-type asteroids. We adopted $m = 0.015$, the value for C-type asteroids, because the comet nucleus may have optical properties similar to those of C-type asteroids rather than S- or M-type asteroids. Substituting $m = 0.015$ and $\alpha = 27.6^\circ$, we obtained an axis ratio of 1:1.25.

The magnitude is related to the effective (or mean) radius of the nucleus, r_n , by

$$p_R \Phi(\alpha) r_n^2 = 2.25 \times 10^{22} r_h^2 \Delta^2 10^{-0.4(m_R - m_\odot)}, \quad (2)$$

where p_R is the geometric albedo in the R_C band; $\Phi(\alpha)$ is the phase function; r_h and Δ are the heliocentric and geocentric distances, respectively, in au; and $m_\odot = -27.1$ is the apparent R_C magnitude of the Sun. $\Phi(\alpha)$ is often assumed to be $\Phi(\alpha) = 10^{-0.4b\alpha}$, where b is a parameter characterizing the phase slope (Belskaya & Shevchenko 2000). We assumed $b = 0.04 \text{ mag deg}^{-1}$ and $p_R = 0.05$, and obtained the R_C band absolute magnitude $H_R = 16.24$ and $r_n = 1.4 \text{ km}$, or the dimension of $2.5 \times 3.2 \text{ km}$. Although there are uncertainties in b (from 0.035 to $0.045 \text{ mag deg}^{-1}$, Belskaya et al. 2000) and p_R (from 0.03 to 0.07 , Kim et al. 2014), which cause a 40% error ($\sim 1 \text{ km}$) in the size, the derived size is in good agreement with that determined by a radar observation¹, which reported dimensions of $2.4 \times 3.0 \text{ km}$. The similarity may suggest that the comet was inactive on 2014 February 1 and has optical properties typical of comet nuclei. For comparison, We fit our data at low phase angle ($\alpha < 40.8^\circ$) using the $H-G$ formalism (Lumme et al. 1984; Bowell et al. 1989) when the comet was apparently inactive, and obtained $H_R = 16.11 \pm 0.26$ and $G = 0.15 \pm 0.17$.

¹<http://www.usra.edu/news/pr/2014/comet209PLINEAR/>

3.3. Coma Photometry

Figure 3 (a) shows the R_C -band reduced magnitude (a hypothetical magnitude observed at 1 au from both the Earth and the Sun) with respect to the phase angle. We set the aperture size for photometry to 3 times the FWHM of point sources ($5''$ – $9''$, depending on the sky conditions). In the figure, we considered the uncertainty of the magnitude on the basis of two factors: one is associated with the uncertainty of the magnitudes of comparison stars (0.25 mag for USNO-A2.0), and the other results from the rotation of the nucleus (a half amplitude of the lightcurve, 0.18 mag), because most of our data could not cover an adequate rotational phase (except the data from UH2.2m and NO1.6m). The data taken on UT 2014 February 01 ($\alpha = 27.6^\circ$) have the smallest error not only because they were calibrated with appropriate standard stars in the Landolt catalog, but also because the data covered a substantial rotational phase for deriving the mean magnitude. In Figure 3 (a), we show the reference magnitude of the nucleus, which is given by $m_R(\alpha) = 16.24 + 0.04\alpha$, following the result in Section 3.2. The magnitude of 209P was significantly brighter than the predicted nuclear magnitude at $\alpha \gtrsim 50^\circ$. Since we considered the rotational brightening/darkening in the error bars, it is unlikely that the magnitude enhancement was caused by sampling bias. When we force fitted the magnitude data with a linear function, we obtained a phase slope of $b = 0.03$, which is inconsistent with low-albedo objects (see Belskaya & Shevchenko 2000). Therefore, it is reasonable to think that the magnitude enhancement was caused by a dusty coma near the nucleus.

Figure 3 (b) and (c) show the differences in magnitude between the observation and the nucleus model with respect to true anomaly θ_T and the heliocentric distance r_h , respectively. There seems to be a weak trend that the residual increased toward perihelion [see Figure 3 (c)]. The magnitude enhancement appears at $r_h = 1.2$ – 1.4 au (or $\theta_T = 285$ – 300°), although the tail was not obvious in our composite images. We conjecture that the nuclear magnitude was brightened at $r_h = 1.2$ – 1.4 au because of a thin dusty coma, although it was not noticeable in our images. It is thus likely that the tail-like feature in Figure 1 (b) could be a dust tail associated with weak comet-like activity (see 3.1). We also noticed that the comet’s activity may not be symmetric with respect to perihelion. The differential magnitude has a peak at $\theta_T \sim 340^\circ$, which is close to perihelion but slightly shifted toward the inbound orbit. Generally, activity peaks of comets tend to shift toward the post-perihelion passages (see, e.g., Ferrín 2010). We conjecture that the activity peak prior to the perihelion may be associated with the seasonal variation of solar incident flux at a localized active region, as indicated for 9P/Tempel 1 (Schleicher 2007).

3.4. Dust Tail and Meteoroid Ejection

To link a comet with a meteor shower, it is important to know how meteoric particles were ejected from the nucleus. We determine the size and ejection velocity using a simple but straightforward method shown below.

We noticed that the edge-on image provides a unique opportunity for deriving the size and ejection velocity. It was taken on UT 2014 May 23 [Figure 1 (d)] in a nearly edge-on view; that is, the angle between the observer and the 209P orbital plane was 3° . Figure 4 shows the surface brightness (Σ) profile of the dust tail integrated within a width of $3'$ perpendicular to the projected orbit, as a function of the distance from the nucleus, d . The profile at $d \lesssim 6''$ was contaminated by light from the nucleus. Since the comet moved rapidly on the sky plan ($12' \text{ min}^{-1}$), it was elongated up to $8''$ by inadequate tracking of the telescope.

In Figure 4, we found that an inflection point exists at $d \sim 50''$. The surface brightness along the tail is consistent with $\Sigma \propto d^\gamma$, where $\gamma = -0.57 \pm 0.05$ at $d = 10''\text{--}50''$ and $\gamma = -0.73 \pm 0.03$ at $d = 50''\text{--}300''$. Because the difference in γ is significant to the accuracy of our measurement, we attribute the discontinuity at $d \sim 50''$ to a discontinuous distribution of dust particles. When dust particles are ejected at a constant rate over a long interval, the resulting steady-state flow of dust particles yields a surface brightness distribution with $\gamma = -0.5$. The similarity in γ values between the observed data at $d = 10''\text{--}50''$ and a steady-state flow suggests that dust particles flowed steadily owing to solar radiation pressure near the nucleus ($d < 50''$). In contrast, the steeper slope beyond $d = 50''$ may suggest that only smaller particles reach the region, as considered in Jewitt et al. (2014). Assuming that the dust particles were ejected after late March at a constant rate, $d < 50''$ corresponds to $\beta > 3 \times 10^{-5}$ or $a \lesssim 1 \text{ cm}$ (a density of $\rho=1 \text{ g cm}^{-3}$ is assumed), where β is again the ratio of the solar radiation pressure acceleration to solar gravity. We adopted the continuous dust ejection model in Jewitt et al. (2014) and found that the dust particles have a differential power-law size distribution with index $q \sim 3.25 \pm 0.10$. The ejection velocity perpendicular to the orbital plane was 0.7 m sec^{-1} for 1-cm grains. Assuming that dust particles were ejected symmetrically to the comet–Sun vector within a half opening angle of $30\text{--}60^\circ$, the net ejection velocity is estimated to be $0.8\text{--}1.4 \text{ m s}^{-1}$. With the model, we also estimated the ejection velocity of 1-mm particles as $2.5\text{--}4.4 \text{ m s}^{-1}$. The velocity is consistent with or slightly faster than the escape velocity (1.4 m s^{-1}) from an 1850-m body with a nuclear mass density of 1 g cm^{-3} . Assuming that the dust has the same optical properties as the nucleus, we derived a total dust grain mass of $(2\text{--}8) \times 10^7 \text{ kg}$. Assuming that the particles were ejected for three months, from late March until late May, we obtained an average mass loss rate around perihelion of $2\text{--}10 \text{ kg s}^{-1}$. The model predicts a loss of 2×10^8 particles s^{-1} for $>1\text{-mm}$ particles. There seems to be an uncertainty of 3–5 times in the particle size

due to the uncertain onset time of the active phase (i.e., late February or late March) and mass density ($0.3\text{--}2\text{ g cm}^{-3}$). The uncertainty is translated into an uncertainty of 3–5 in the particle production rate. Considering all of the results above, we concluded that meteoric particles (1–10 mm) were marginally ejected from the highly dormant comet nucleus via gas outflow only when the comet was around perihelion.

The peak activity of the Camelopardalids occurred on UT 2014 May 24 as predicted. Brown (2014) reported that the shower signals were dominated by small particles of milligram mass and smaller (i.e. $\lesssim 1\text{ mm}$). Further research is needed to connect the observed mass ejection for 209P and meteor shower, taking account of dynamical evolution (Vaubaillon & Colas 2005) and probably fragmentation of dust aggregates (Madiedo et al. 2014).

4. Summary

We made observations of 209P during its perihelion passage in 2014 and found the following:

1. 209P/LINEAR was apparently inactive at the heliocentric distance $r_h = 1.6\text{ au}$ and showed weak activity at $r_h \leq 1.4\text{ au}$.
2. The observed morphology is similar in the R_C and I_C bands, suggesting that scattered sunlight from the nucleus and dust particles was the dominant light source at these optical wavelengths.
3. The comet was determined to have a negligibly small active fraction ($<0.001\%$) based on upper limit coma measurements made prior to the appearance of clear cometary activity.
4. During the active phase, it ejected dust particles up to 1 cm in size with a differential power-law size distribution with index $q = -3.25 \pm 0.10$.
5. The total ejected dust mass and average mass loss rate were $(2\text{--}8) \times 10^7\text{ kg}$ and $2\text{--}10\text{ kg sec}^{-1}$, respectively.

Acknowledgments

This research was conducted as part of a joint research project titled “Recherche sur les liens entre comètes et météores.” MI was supported by the Paris Observatory during his stay in

Paris (2014 May–July). This research was also supported by a National Research Foundation of Korea (NRF) grant funded by the Korean government (MEST) (No. 2012R1A4A1028713). The observations at OAO, IAO, NHAO, and NO were supported by the Optical and Near-infrared Astronomy Inter-University Cooperation Program and Grants-in-Aid for Scientific Research (23340048, 24000004, 24244014, and 24840031) from the Ministry of Education, Culture, Sports, Science and Technology of Japan. TRAPPIST is a project funded by the Belgian Fund for Scientific Research (Fonds National de la Recherche Scientifique, F.R.S.-FNRS). C. Opitom acknowledges the support of the FNRS. E. Jehin and M. Gillon are FNRS Research Associates. SH was supported by the Space Plasma Laboratory, ISAS, JAXA.

REFERENCES

- Belskaya, I. N., & Shevchenko, V. G. 2000, *Icarus*, 147, 94
- Bowell, E., Hapke, B., Domingue, D., et al. 1989, *Asteroids II*, 524
- Brown, M. E., Bouchez, A. H., Spinrad, A. H., & Johns-Krull, C. M. 1996, *AJ*, 112, 1197
- Brown, P. 2014, *Central Bureau Electronic Telegrams*, 3886, 1
- Ferrín, I. 2010, *Planet. Space Sci.*, 58, 365
- Finson, M., & Probst, R. 1968, *ApJ*, 154, 327
- Green, D. W. E. 2014, *Central Bureau Electronic Telegrams*, 3881, 1
- Holmberg, J., Flynn, C., & Portinari, L. 2006, *MNRAS*, 367, 449
- Ishiguro, M., Sarugaku, Y., Ueno, M., Miura, N., Usui, F., Chun, M.-Y., & Kwon, S. M. 2007, *Icarus*, 189, 169
- Ishiguro, M., Ham, J.-B., Tholen, D. J., et al. 2011, *ApJ*, 726, 101
- Ishiguro, M., Kim, Y., Kim, J., et al. 2013, *ApJ*, 778, 19
- Ivezić, Ž., Smith, J. A., Miknaitis, G., et al. 2007, *AJ*, 134, 973
- Jehin, E., Gillon, M., Queloz, D., et al. 2011, *The Messenger*, 145, 2
- Jenniskens, P., & Lytinen, E. 2014, *Central Bureau Electronic Telegrams*, 3869, 1
- Jewitt, D. C., & Meech, K. J. 1987, *ApJ*, 317, 992

- Jewitt, D. C. 2002, *AJ*, 123, 1039
- Jewitt, D., Ishiguro, M., Weaver, H., et al. 2014, *AJ*, 147, 117
- Kim, J., Ishiguro, M., Hanayama, H., et al. 2012, *ApJ*, 746, L11
- Landolt, A. U. 1992, *AJ*, 104, 1, 340
- Lumme, K., Bowell, E., & Harris, A. W. 1984, *BAAS*, 16, 684
- Luu, J. X., & Jewitt, D. C. 1992, *Icarus*, 97, 276
- Madiedo, J. M., Trigo-Rodríguez, J. M., Zamorano, J., et al. 2014, *MNRAS*, 445, 3309
- Mothé-Diniz, T., Carvano, J. M. Á., & Lazzaro, D. 2003, *Icarus*, 162, 10
- Schleicher, D. G. 2007, *Icarus*, 191, 322
- Skrutskie, M. F., Cutri, R. M., Stiening, R., et al. 2006, *AJ*, 131, 1163
- Schleicher, D. 2014, *Central Bureau Electronic Telegrams*, 3880, 1
- Tancredi, G., Fernández, J. A., Rickman, H., & Licandro, J. 2006, *Icarus*, 182, 527
- Vaubaillon, J., & Colas, F. 2005, *A&A*, 431, 1139
- Watanabe, M., Takahashi, Y., Sato, M., et al. 2012, *Proc. SPIE*, 8446,
- Ye, Q., & Wiegert, P. A. 2014, *MNRAS*, 437, 3283
- Zappala, V., Cellino, A., Barucci, A. M., Fulchignoni, M., & Lupishko, D. F. 1990, *A&A*, 231, 548

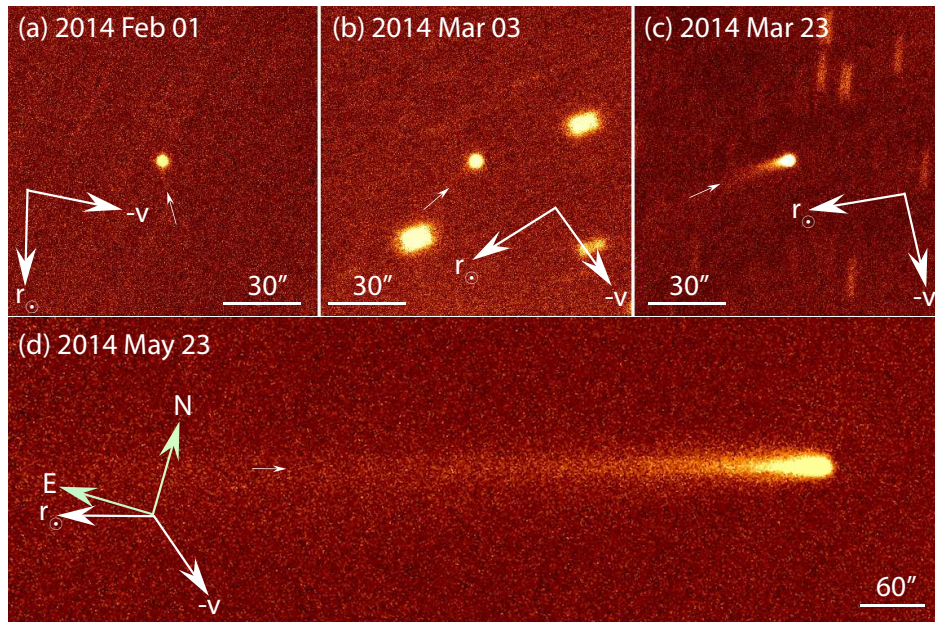


Fig. 1.— Selected images of 209P. The top three images (a–c) have the standard orientation in the sky: north is up, and east is to the left, and the bottom image (d) is rotated by -17° so that the Sun–comet vector is parallel to the horizontal axis. The FOV is $2' \times 2'$ (a–c) and $14.5' \times 4.8'$ (d). The antisolar direction (r_{\odot}) and the negative heliocentric velocity vector ($-v$) are shown by arrows. Thin arrows indicate possible dust tails.

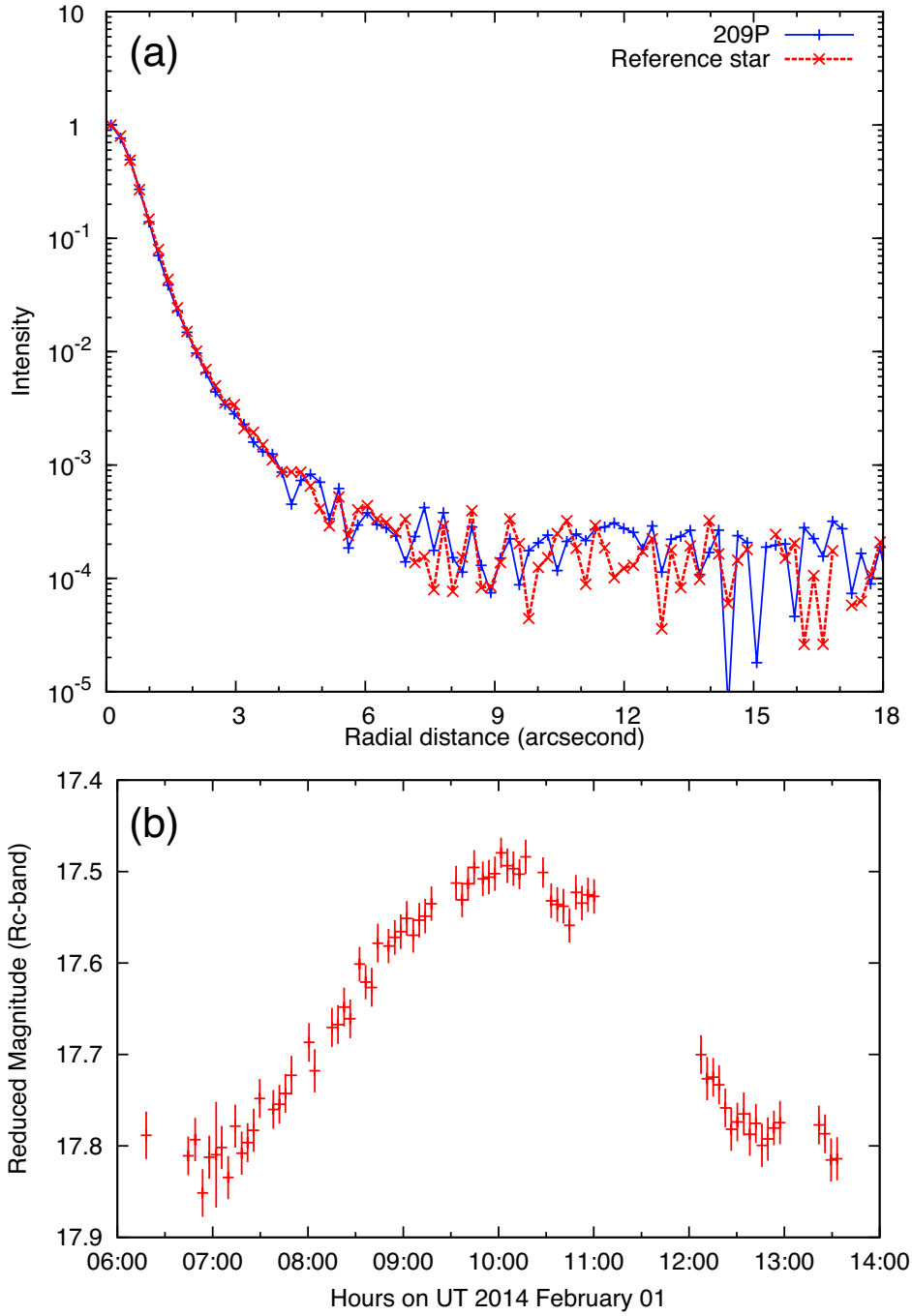


Fig. 2.— (a) Normalized surface brightness profiles of 209P (solid line) and a reference star (dashed line) taken on UT 2014 February 1. The stellar profile was taken in sidereal tracking mode six times at the beginning, middle and end of 209P exposures with the exposure time of 180 seconds. We could not find a noticeable time-variation in the stellar profiles. (b) Rotational lightcurve on the same night. Vertical axis denotes the reduced magnitude, and horizontal axis denotes UT on 2014 February 01 after light time correction.

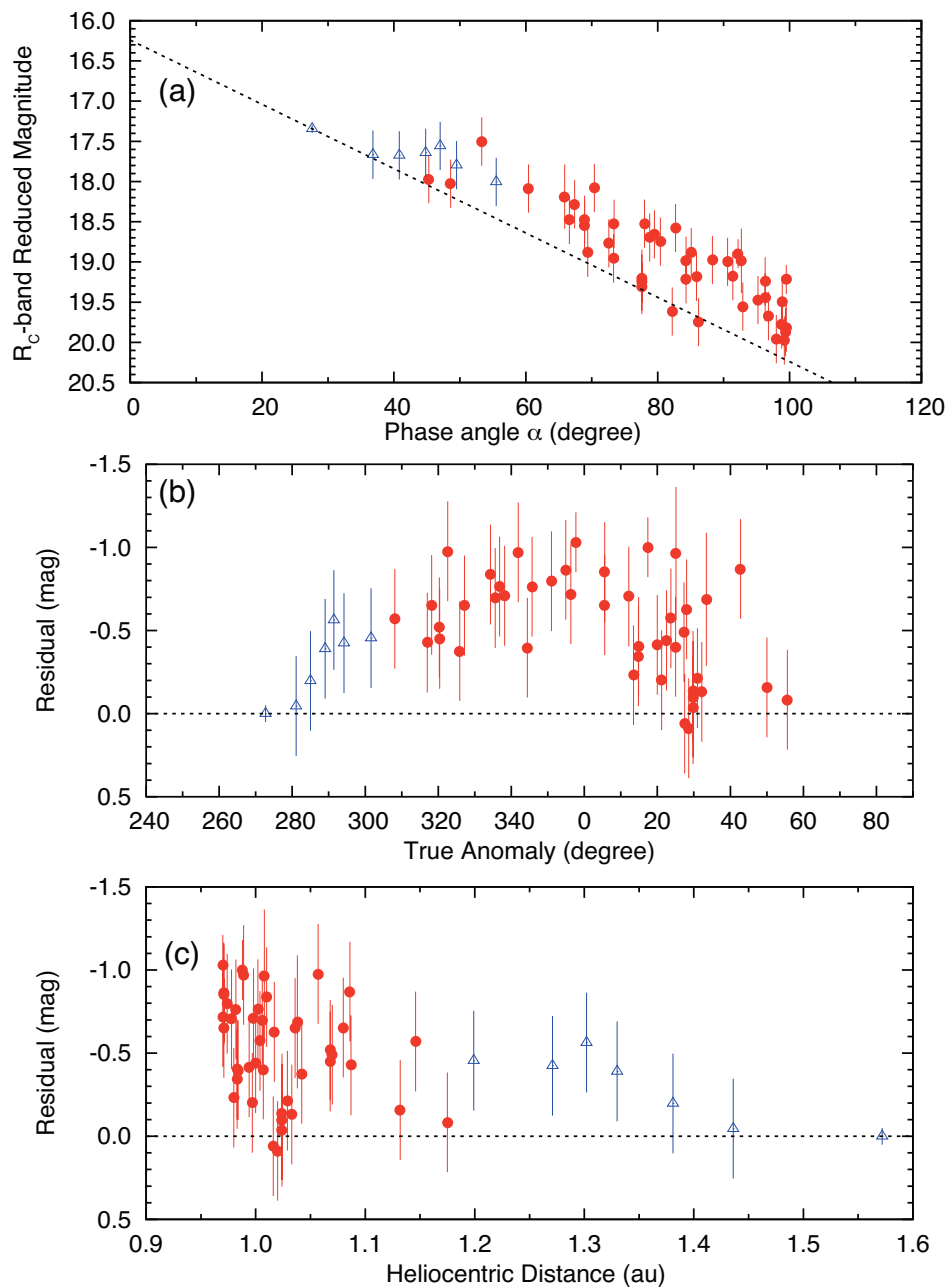


Fig. 3.— Photometric results: (a) Magnitude–phase relation of 209P/LINEAR. Dashed line denotes the predicted mean magnitude of the rotating nucleus. (b) Residual of magnitudes after subtraction of the nuclear contribution with respect to the true anomaly θ_T . (c) Residual of magnitudes with respect to the distance from the Sun. Open triangles are magnitudes when the comet showed obvious tail while filled circles are magnitude when the comet appeared point-like.

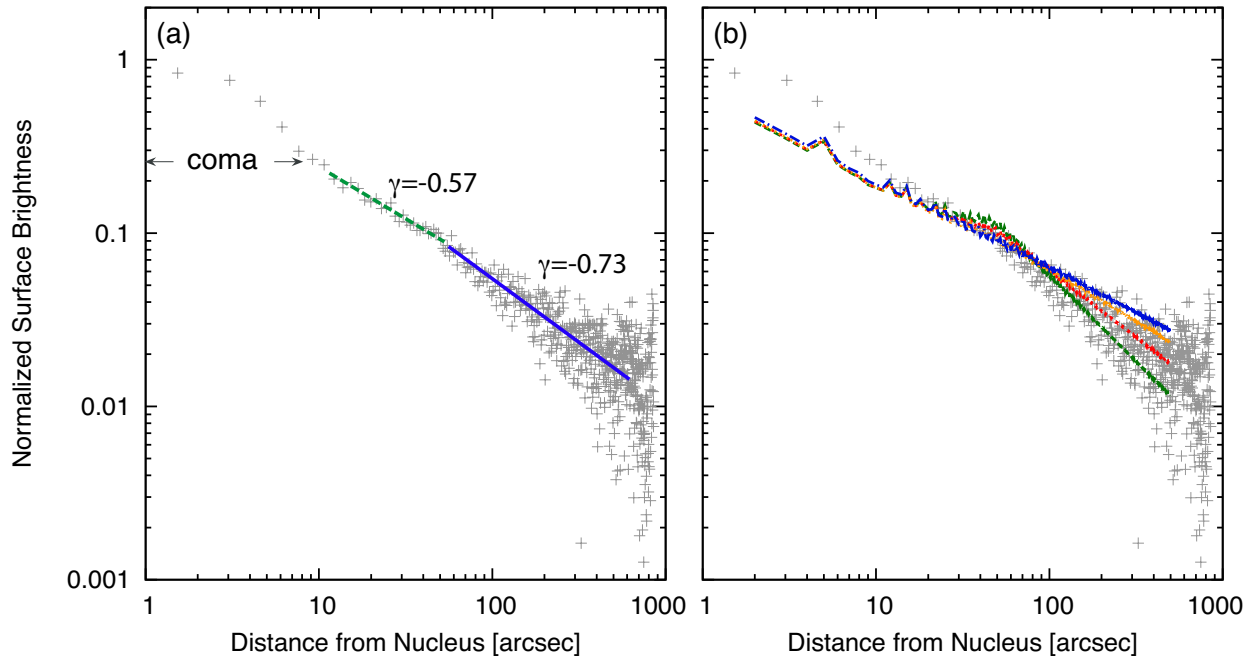


Fig. 4.— Surface brightness profiles of 209P (crosses) with respect to distance from the nucleus observed on UT 2014 May 23. (a) The profile was fitted by power-law functions with indexes $\gamma = -0.57$ ($d = 10''\text{--}50''$) and $\gamma = -0.73 \pm 0.03$ ($d = 50''\text{--}300''$). (b) Model profiles in which dust is ejected continuously starting on UT 2014 February 22. We assumed the minimum β ($= 3 \times 10^{-5}$), which corresponds to 1-cm grains, to produce the observed inflection point at $d \sim 50''$. The power-law indices are $q = -3.75$ (blue), -3.50 (orange), -3.25 (red), and -3.00 (green) from top to bottom.

Table 1. Observation summary

Median UT	Telescope	Filter	N^a	T_{tot}^b	r_h^c	Δ^d	α^e	f_T^f	Mag ^g	Tail ^h
2014-Feb-01.418	UH 2.2 m	R _C	72	216	1.572	0.729	27.6	272.7	17.6	No
2014-Feb-16.540	IAO 1.0 m	g', R _C , I _C	17	51	1.436	0.663	36.8	281.1	17.6	No
2014-Feb-22.697	IAO 1.0 m	g', R _C , I _C	17	51	1.381	0.641	40.8	285.0	17.4	No
2014-Feb-28.598	IAO 1.0 m	g', R _C , I _C	19	57	1.330	0.622	44.8	289.0	17.2	No
2014-Mar-03.855	NHAO 2.0 m	R _C	20	10	1.302	0.611	47.0	291.4	17.1	No
2014-Mar-07.641	NHAO 2.0 m	R _C	55	27.5	1.271	0.598	49.5	294.2	17.2	No
2014-Mar-16.551	IAO 1.0 m	g', R _C , I _C	11	33	1.199	0.565	55.5	301.6	17.2	No
2014-Mar-22.604	IAO 1.0 m	g', R _C , I _C	24	72	1.154	0.539	59.6	307.1	–	Yes
2014-Mar-23.660	NHAO 2.0 m	R _C	45	90	1.146	0.534	60.4	308.1	17.0	Yes
2014-Apr-01.502	OAO 0.5 m	g', R _C , I _C	53	53	1.087	0.488	66.6	317.0	17.1	Yes
2014-Apr-02.618	NHAO 2.0 m	R _C	14	28	1.080	0.481	67.4	318.2	16.9	Yes
2014-Apr-04.562	IAO 1.0 m	g', R _C , I _C	18	54	1.068	0.470	68.9	320.3	17.0	Yes
2014-Apr-04.620	NHAO 2.0 m	R _C	20	40	1.068	0.470	68.9	320.4	17.1	Yes
2014-Apr-06.643	NHAO 2.0 m	R _C	41	82	1.057	0.457	70.4	322.6	16.5	Yes
2014-Apr-09.514	OAO 0.5 m	g', R _C , I _C	55	55	1.042	0.439	72.6	325.9	17.1	Yes
2014-Apr-10.596	IAO 1.0 m	g', R _C , I _C	20	60	1.036	0.432	73.4	327.2	16.8	Yes
2014-Apr-16.534	NHAO 2.0 m	R _C	20	40	1.010	0.390	78.0	334.3	16.5	Yes
2014-Apr-17.610	IAO 1.0 m	g', R _C , I _C	18	54	1.006	0.382	78.8	335.6	16.6	Yes
2014-Apr-18.547	NHAO 2.0 m	R _C	30	60	1.002	0.375	79.5	336.8	16.5	Yes
2014-Apr-19.638	NHAO 2.0 m	R _C , I _C	30	60	0.998	0.366	80.4	338.2	16.6	Yes
2014-Apr-22.549	NHAO 2.0 m	R _C	32	63	0.989	0.343	82.7	341.9	16.2	Yes
2014-Apr-24.503	OAO 0.5 m	g', R _C , I _C	36	72	0.984	0.328	84.3	344.4	16.8	Yes
2014-Apr-25.544	NHAO 2.0 m	R _C	40	40	0.982	0.319	85.1	345.7	16.4	Yes
2014-Apr-29.572	IAO 1.0 m	g', R _C , I _C	11	33	0.974	0.286	88.3	351.0	16.2	Yes
2014-May-02.486	OAO 0.5 m	g', R _C , I _C	36	72	0.971	0.260	90.6	354.9	16.0	Yes
2014-May-03.584	NHAO 2.0 m	R _C	40	80	0.970	0.251	91.4	356.3	16.1	Yes
2014-May-04.610	NO 1.6 m	R _C	11	17	0.970	0.242	92.2	357.7	15.8	Yes
2014-May-10.491	OAO 0.5 m	g', R _C , I _C	36	72	0.971	0.190	96.3	5.6	15.8	Yes
2014-May-10.534	NHAO 2.0 m	R _C	27	40.5	0.971	0.190	96.3	5.6	15.6	Yes
2014-May-15.531	NHAO 2.0 m	R _C	11	16.5	0.978	0.145	98.9	12.2	15.3	Yes
2014-May-16.542	NHAO 2.0 m	R _C	40	60	0.980	0.136	99.2	13.5	15.6	Yes
2014-May-17.486	OAO 0.5 m	g', R _C , I _C	45	45	0.983	0.128	99.4	14.8	15.4	Yes
2014-May-17.541	NHAO 2.0 m	R _C	39	58.5	0.983	0.127	99.5	14.9	15.3	Yes
2014-May-19.888	NO 1.6 m	R _C	12	8	0.988	0.110	99.5	17.4	14.4	Yes
2014-May-21.547	OAO 0.5 m	g', R _C , I _C	193	96.5	0.994	0.094	98.8	20.0	14.6	Yes
2014-May-22.508	OAO 0.5 m	g', R _C , I _C	73	73	0.997	0.087	98.0	21.2	14.6	Yes
2014-May-23.541	OAO 0.5 m	g', R _C , I _C	167	167	1.000	0.079	96.8	22.5	14.2	Yes
2014-May-24.491	OAO 0.5 m	g', R _C , I _C	26	26	1.004	0.073	95.2	23.7	13.8	Yes
2014-May-25.504	OAO 0.5 m	g', R _C , I _C	51	51	1.007	0.067	92.9	25.0	13.7	Yes
2014-May-25.586	IAO 1.0 m	g', R _C , I _C	11	33	1.008	0.066	92.7	25.1	13.1	Yes
2014-May-27.522	OAO 0.5 m	g', R _C , I _C	230	115	1.070	0.058	85.9	27.3	13.2	Yes
2014-May-27.535	NHAO 2.0 m	R _C	92	23.25	1.016	0.058	86.2	27.5	13.1	Yes
2014-May-28.006	TRAPPIST 0.6 m	R _C	2	6	1.017	0.057	84.3	28.0	12.7	Yes
2014-May-28.477	OAO 0.5 m	g', R _C , I _C	18	9	1.020	0.056	82.2	28.6	13.4	Yes
2014-May-29.497	OAO 0.5 m	g', R _C , I _C	52	26	1.024	0.055	77.6	29.8	13.0	Yes
2014-May-29.504	IAO 1.0 m	g', R _C , I _C	46	23	1.024	0.056	77.6	29.8	13.0	Yes

Table 1—Continued

Median UT	Telescope	Filter	N^a	T_{tot}^b	r_h^c	Δ^d	α^e	f_T^f	Mag ^g	Tail ^h
2014-May-29.513	NHAO 2.0 m	R _C	105	26.25	1.024	0.056	77.6	29.8	13.1	Yes
2014-May-30.489	OAO 0.5 m	g', R _C , I _C	102	51	1.029	0.057	73.3	31.0	12.7	Yes
2014-May-31.478	OAO 0.5 m	g', R _C , I _C	52	26	1.033	0.059	69.4	32.2	12.8	Yes
2014-Jun-01.506	IAO 1.0 m	g', R _C , I _C	7	3.5	1.038	0.064	65.9	33.4	12.1	Yes
2014-Jun-10.028	TRAPPIST 0.6 m	R _C	1	1	1.086	0.127	53.2	42.9	13.2	Yes
2014-Jun-16.990	TRAPPIST 0.6 m	R _C	5	5	1.132	0.191	48.6	50.0	14.7	Yes
2014-Jun-24.028	TRAPPIST 0.6 m	R _C	6	6	1.183	0.258	44.8	56.6	15.3	Yes

^aNumber of exposures

^bTotal exposure time (min)

^cHeliocentric distance (au)

^dGeocentric distance (au)

^eSolar phase angle (degree)

^fTrue anomaly (degree)

^gR_C-band magnitudes

^hIs a tail clearly observed?